# Electron Doping of $Ca_4Mn_3O_{10}$ Induced by Vanadium Substitution

M. D. Carvalho,*[,†] R. P. Borges,[‡] A. V. Girão,[†,§] M. M. Cruz,[‡] M. E. Melo Jorge,[†] G. Bonfait,[∥,⊥] P. Dluzewski,[#] and M. Godinho[‡]

*Departamento de Química e Bioquímica/CCMM and Departamento de Física/CFMC-UL, Faculdade de Ciências, Universidade de Lisboa, Campo Grande, 1749-016 Lisboa, Portugal; Departamento de Química, Instituto Tecnológico Nuclear, 2686-953 Sacavém, Portugal; CEFITEC, Departamento Física, Fac. Ciências e Tecnologia, Universidade Nova Lisboa, 2829-516 Caparica, Portugal; and Institute of Physics, Polish Academy of Sciences, Al. Lotnikow 32/46, 02-668, Warsaw, Poland*

*Received February 21, 2005*

In this work, electron doping of the anisotropic phase $Ca_4Mn_3O_{10}$ was achieved by substitution of manganese by vanadium. No significant structural modifications were detected to the highest substitution ratio of 10% achieved. The introduction of vanadium decreases the electrical resistivity, described as two-dimensional variable range hopping, and induces the appearance of a ferromagnetic behavior. Consistently negative magnetoresistance develops in the magnetic ordered state. These results are characteristic of the presence of double exchange interactions, indicating that vanadium doping induces mixed valence of manganese.

## Introduction

Perovskite-related manganese oxides are an important class of materials due to the magnetoresistive properties displayed. Investigations on manganites exhibiting colossal magnetoresistance (CMR) have shown that this effect originates from a double exchange mechanism between $Mn^{3+}$ and $Mn^{4+}$ that promotes ferromagnetic interactions.[1]

Most of the work carried out in the search for optimal compositions has been based on the substitution of the A-cation in the $AMnO_3$ perovskites.[2−5] However, an alternative route to induce CMR in manganese perovskites has been the doping of the Mn sites (B-sites) by other cations, especially with a higher valence, such as Re, Ru, Nb, W, Ta, and Mo.[6−9] For Re and Ru ions, which are mainly pentavalent, the results were explained by valence effects, which lead to the formation of $Mn^{3+}$ in the $Mn^{4+}$ substructure and consequently induce double exchange interactions.[6] For Nb, W, Ta, and Mo doping,[7] the obtained results show that the electron doped manganites $CaMn_{1-x}M_xO_{3-\delta}$ exhibit significant ferromagnetic interactions and CMR at low temperature, associated with a quasi-semimetallic behavior over a wide composition range. These results indicate that the valence of the doping element is relevant for the induction of CMR in $CaMnO_3$.

Ruddlesden−Popper (RP) compounds, with general formula $A_{n+1}B_nO_{3n+1}$, also exhibit magnetoresistivity and are a good choice to study some of the phenomena involved in CMR and/or orbital ordering.

In this work, the substitution of manganese by vanadium in the RP phase $Ca_4Mn_3O_{10}$, which can be described as $(CaMnO_3)_3CaO$ (a perovskite block separated by a rock-salt layer), was undertaken.

The pentavalent vanadium cation was chosen to induce the formation of $Mn^{3+}$ ions in the $Mn^{4+}$ substructure, without significant structural modifications due to the similar ionic radius values (0.54 and 0.53 Å for $V^{5+}$ and $Mn^{4+}$, respectively).[10]

## Experimental Section

Samples of $Ca_4Mn_{3-x}V_xO_{10}$ ($x = 0$, 0.1, 0.2, and 0.3) were prepared by a citrate gel technique. Attempts to obtain higher contents of Mn substitution led to multiphase samples. Stoichiometric amounts of $CaCO_3$ (99.95%), $Mn(NO_3)_2{\cdot}4H_2O$ (>98%), and $V_2O_5$ (>99%) were separately dissolved in $HNO_3$, to which was added citric acid and urea (in an amount equal to the total metal ions). The solution was heated on a sand bath, resulting in the formation and degradation of a gel. The products were heated at 773 K for 4 h in order to remove the organic matter and to decompose the nitrates. The resulting amorphous powders were heated at 1573 K, in air, for several days, with intermittent grinding.

Structural characterization by X-ray diffraction (XRD) was carried out for all samples, using a Philips PW 1730 X-ray powder diffractometer, operating with Cu Kα radiation. The analysis of the XRD data was carried out with the Fullprof program[11] using a polynomial function to model the background level and describing the peak shape with pseudo-Voight functions and two asymmetry

* Corresponding author. E-mail: mdcarvalho@fc.ul.pt.
† Departamento de Química e Bioquímica/CCMM, Universidade de Lisboa.
‡ Departamento de Física/CFMC-UL, Universidade de Lisboa.
§ Present address: Civil Engineering Materials Unit, School of Civil Engineering, University of Leeds, Leeds LS2 9JT, UK.
∥ Instituto Tecnológico Nuclear.
⊥ University Nova Lisboa.
# Polish Academy of Sciences.

(1) Zenner, C. *Phys. Rev.* **1951**, *82*, 403.
(2) Mahesh, R.; Mahendiran, R.; Raychaudhuri, A. K.; Rao, C. N. R. *J. Solid State Chem.* **1995**, *114*, 297.
(3) von Helmot, R.; Wecker, J.; Holzapfel, B.; Schultz, L.; Samwer, K. *Phys. Rev. Lett.* **1993**, *71*, 2331.
(4) Martin, C.; Maignan, A.; Damay, F.; Hervieu, M.; Raveau, B. *J. Solid State Chem.* **1997**, *134*, 198.
(5) Rao, C. N. R.; Santosh, A. P. N.; Cheetham, A. K. *Chem. Mater.* **1998**, *10*, 2714.
(6) Raveau, B.; Maignan, A.; Martin, C.; Hervieu, M. *Mater. Res. Bull.* **2000**, *35*, 1579.
(7) Raveau, B.; Zhao, Y. M.; Martin, C.; Hervieu, M.; Maignan, A. *J. Solid State Chem.* **2000**, *149*, 203.
(8) Maignan, A.; Martin, C.; Hervieu, M.; Raveau, B. *Solid State Commun.* **2001**, *117*, 377.
(9) Vanitha, P. V.; Arulraj, A.; Raju, A. R.; Rao, C. N. R. *C. R. Acad. Sci. Paris* **1999**, t.2, Série II C, 595.
(10) Shannon, R. D.; Prewitt, C. T. *Acta Crystallogr.* **1969**, *B25*, 925.
(11) Rodriguez-Carvajal, J. *Fullprof*, version 1.8a, May 2002, ILL (unpublished).

10.1021/cm050395r CCC: $30.25 
Published on Web 08/25/2005

parameters. The occupancy factors were fixed according to the sample stoichiometry, and a correction for preferred orientation was included in the refinement.

TEM investigations were made using a JEM 2000EX microscope operating at 200 kV. The specimens for TEM were powered in an agate mortar, ultrasonically dispersed in butyl alcohol and deposited onto holey carbon film supported on 300 mesh copper grid. The diffraction patterns were interpreted with the aid of EMS software package.[12] Electron dispersive X-ray analysis (EDX) were performed on randomly selected crystallites to verify the homogeneity of the samples, using a JEM3010 microscope attached with energy-dispersive X-ray spectroscopy (EDS), using a 10 nm nanobeam with 300 kV accelerating voltage.

Magnetization as a function of temperature and magnetic field was measured in a SQUID magnetometer. Electrical resistivity measurements were carried out on bar-shaped bulk samples, using an in-line four-point contact geometry and a dc current ranging from 1 $\mu$A to 1 mA, for temperatures between 5 and 300 K, under magnetic fields up to 16 T.

## Results and Discussion

XRD data and the results of Rietveld refinements are presented in Figure 1 for the $x = 0.1$, 0.2, and 0.3 samples, respectively. All samples were refined on the basis of an orthorhombic $Ca_4Mn_3O_{10}$ type structure (space group *Pbca*), considering a statistical distribution of Mn and V cations on the two independent crystallographic sites, based on nominal composition. The initial positional parameters were taken from previous reported data of $Ca_4Mn_3O_{10}$.[13] All the peaks can be assigned to the $n = 3$ Ruddlesden−Popper phase. The relatively high residual values obtained for the samples and the intensity difference observed on some peaks can be ascribed to the presence of intergrowth phenomena, as previously observed by other authors.[13−16]

The *Pbca* structure derived from X-ray diffraction was confirmed by the electron diffraction investigation of all the samples. In Figure 2 we present some experimental and calculated ED patterns of the $Ca_4Mn_{2.8}V_{0.2}O_{10}$ sample. The experimental and calculated patterns are in good agreement. Only some differences in spot intensities could be observed, but this discrepancy can be explained by the double diffraction effect. Reflection conditions for space group *Pbca* are fulfilled for the ($h$00), (0$k$0), and (00$l$) reflections (respectively, $h = 2n$, $k = 2n$, and $l = 2n$). The absence of (00$l$) reflections with odd $l$ proved that the structure of the investigated samples is free of twins, previously reported for $Ca_4Mn_3O_{10}$.[17]

The high-resolution electron microscopy (HRTEM) images also confirmed the *Pbca* structure for the investigated samples with some intergrowth defects along the $c$ axis. As an example, a disturbance in the stacking of $a-b$ planes for the $Ca_4Mn_{2.9}V_{0.1}O_{10}$ sample is presented in Figure 3, where the image and diffraction pattern were taken with an electron beam nearly parallel to the $b$-axis. On the image, several nanometer wide strips separate regions with well-established periodical array of fringes where the spacing of ~13 Å corresponds to the interplanar distance $d_{002}$. Probably, the separating strips possess a perovskite structure. The observation of intergrowth defects supports the explanation for the discrepancies between experimental and calculated peak intensities of the XRD refinements.

EDX analysis was performed on preselected crystallites of the well-formed RP phases as well as on some regions where intergrowth defects could be identified. Vanadium was

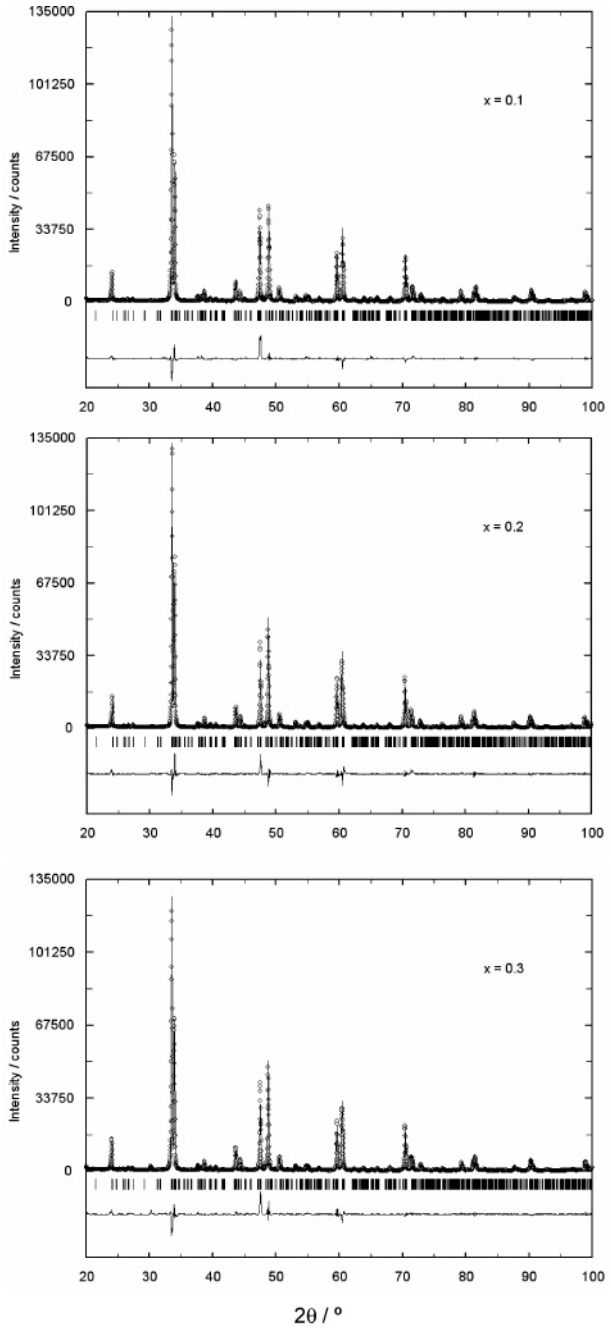


**Figure 1.** Observed and calculated (solid line) Rietveld refinement plot of the XRD patterns for $Ca_4Mn_{3-x}V_xO_{10}$. The difference plot is at the bottom of the figure and tick marks represent allowed reflections. (Residual values obtained: $R_{wp} = 15.8\%$, $R_P = 12.6\%$, $R_B = 9.88$ for $x = 0.1$; $R_{wp} = 15.5\%$, $R_P = 12.4\%$, $R_B = 7.90$ for $x = 0.2$; and $R_{wp} = 14.6\%$, $R_P = 12.0$, $R_B = 7.87$ for $x = 0.3$).

(12) Stadelman, P. A. *Ultramicroscopy* **1987**, *21*, 131.
(13) Sousa, P. M.; Girão, A. V.; Melo Jorge, M. E.; Carvalho, M. D.; Costa, F. M.; Borges, R. P.; Cruz, M. M.; Godinho, M. *J. Phys. Chem. Solids* **2004**, *65*, 1823.
(14) Chen, R,; Greenblatt, M.; Bendersky, L. A. *Chem. Mater*. **2001**, *13*, *4094*.
(15) Caldes, M. T.; Goglio, G.; Marhic, C.; Joubert, O.; Lancin, M.; Brohan, L. *Int. J. Inorg. Mater.* **2001**, *3*, 1169.
(16) Lee, J. Y.; Swinnea, J. S.; Steinfink, H.; Reiff, W. M.; Pei, S.; Jorgensen, J. D. *J. Solid State Chem*. **1993**, *103*, 1.

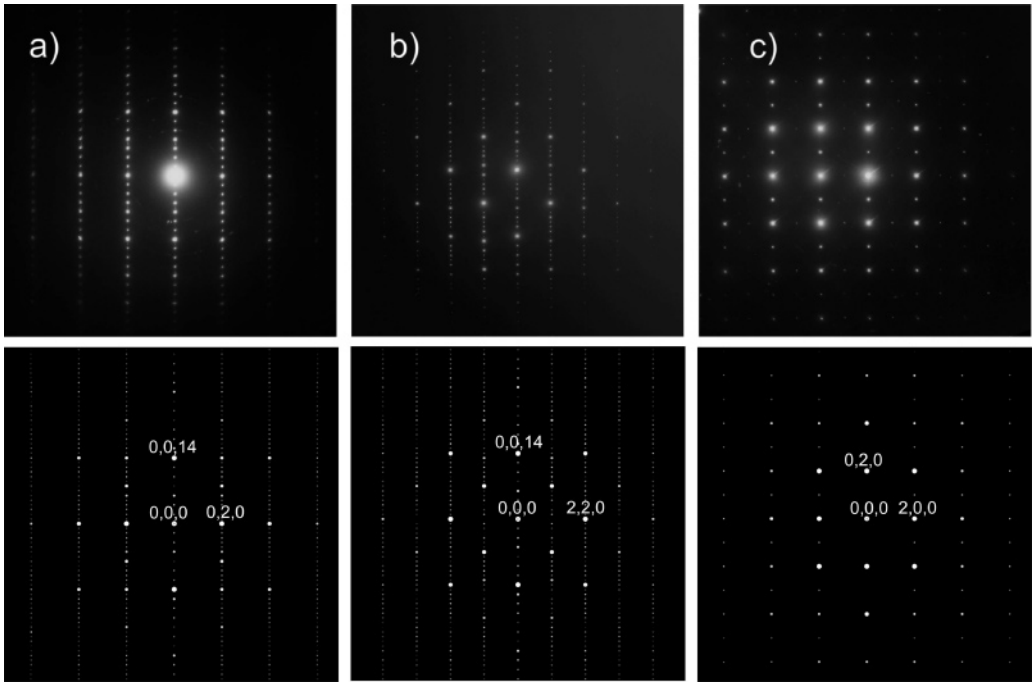


**Figure 2.** Experimental (upper row) and calculated (bottom row) electron diffraction patterns for $Ca_4Mn_{2.8}V_{0.2}O_{10}$ taken with electron beam along (a) [100], (b) [110], and (c) [001].

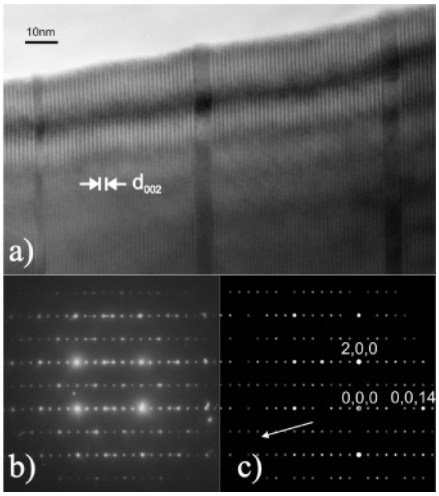


**Figure 3.** (a) HRTEM image and (b) experimental and (c) calculated diffraction patterns of $Ca_4Mn_{2.9}V_{0.1}O_{10}$ sample with electron beam inclined 3° apart from the *b*-axis in the direction indicated by the white arrow.

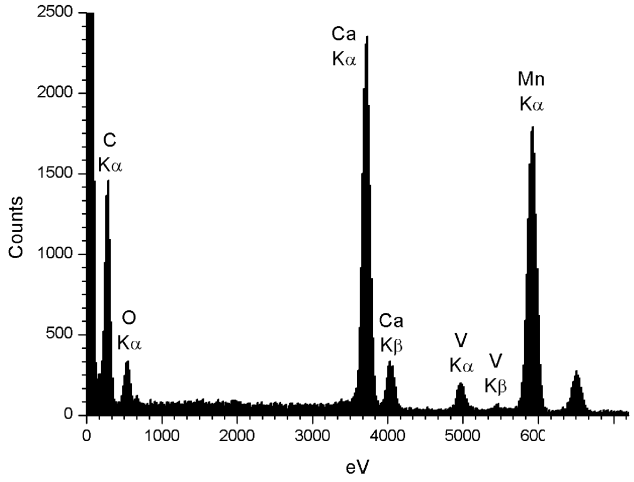


**Figure 4.** EDX spectrum for $x = 0.3$; the C line originates from the supported carbon film.

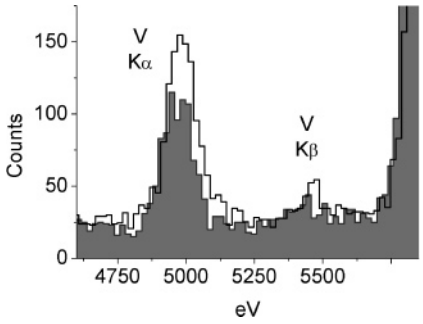


**Figure 5.** Part of the spectra with V lines for samples with $x = 0.1$ (gray area) and 0.3 (solid line). The spectra were normalized to the intensity of Mn Kα.

detected on both regions. Figure 4 presents the global spectra obtained for the $x = 0.3$ sample and Figure 5 part of the obtained spectra with the vanadium lines for the $x = 0.1$ and 0.3 samples of the RP phases. The results establish the presence of vanadium in the RP phases with the V/Mn content ratio values in accordance with the referred composition.

Partial substitution of Mn for V in $Ca_4Mn_3O_{10}$ results in a slight increase of the lattice parameters in the $a-b$ plane and a compression of the $c$ axis for $x = 0.1$ and 0.2 with an overall increase of the cell volume (Table 1). No significant differences were detected between the $x = 0.2$ and 0.3 samples. The nonlinear variation of the cell parameters of the samples with Mn substitution can be understood as resulting from different effects. Considering vanadium ions as $V^{5+}$ (0.54 Å), the substitution should lead to some reduction of $Mn^{4+}$ (0.53 Å) to $Mn^{3+}$ (0.645 Å), which could justify a cell volume increase. However, the existence of oxygen vacancies cannot be disregarded and their presence will also influence the cell parameter values. Oxygen deficiency was previously reported for $Ca_4Mn_3O_{10}$[18] and $Ca_4Mn_2TiO_{9.93}$,[19] and in the latter case, the obtained mean

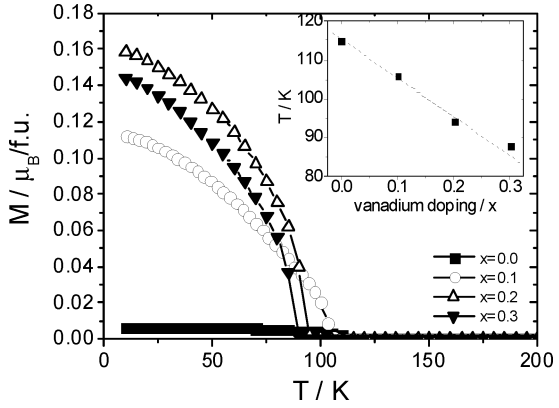


**Figure 6.** Field-cooled magnetization measured at 10 mT for $Ca_4Mn_{3-x}V_xO_{10}$. The inset shows the variation of the critical temperature with V doping.

**Table 1. Cell Parameter Values of the Prepared Samples**

| | *a*/Å | *b*/Å | *c*/Å | *V*/Å$^3$ |
|---|---|---|---|---|
| $Ca_4Mn_3O_{10}$[13] | 5.2602(2) | 5.2568(2) | 26.829(1) | 741.87(5) |
| $Ca_4Mn_{2.9}V_{0.1}O_{10}$ | 5.2724(2) | 5.2671(2) | 26.813(1) | 744.61(4) |
| $Ca_4Mn_{2.8}V_{0.2}O_{10}$ | 5.2829(1) | 5.2764(2) | 26.779(1) | 746.46(3) |
| $Ca_4Mn_{2.7}V_{0.3}O_{10}$ | 5.2832(2) | 5.2756(2) | 26.779(1) | 746.40(4) |

bond length, smaller than expected, was attributed to the influence of oxygen vacancies located on the equatorial anion site of the outer layer of the perovskite. Consequently, we cannot predict the $Mn^{3+}/Mn^{4+}$ ratio using only the vanadium content of the samples. Oxygen deficiency may justify the similar values obtained for the cell volume of $x = 0.2$ and 0.3 samples.

Magnetization measurements as a function of temperature and magnetic field were carried out for all the samples. As previously reported,[20,21] the $x = 0$ compound displays antiferromagnetic (AFM) behavior, with $T_N = 115$ K and a small ferromagnetic component evidenced in the $M(H)$ curves for low applied fields. This component has been attributed to a small canting of the magnetic substructures.[22,23]

Upon V substitution, a ferromagnetic behavior is detected for all samples (Figure 6). Magnetization as a function of magnetic field confirms the presence of a ferromagnetic component that increases with increasing vanadium content (Figure 7). The transition temperature, taken as the inflection point of the temperature dependence of the magnetization, decreases linearly with vanadium doping (inset of Figure 6).

However, all samples exhibit a high magnetic susceptibility at high fields, indicating that the coupling remains essentially antiferromagnetic. This is confirmed by the asymptotic

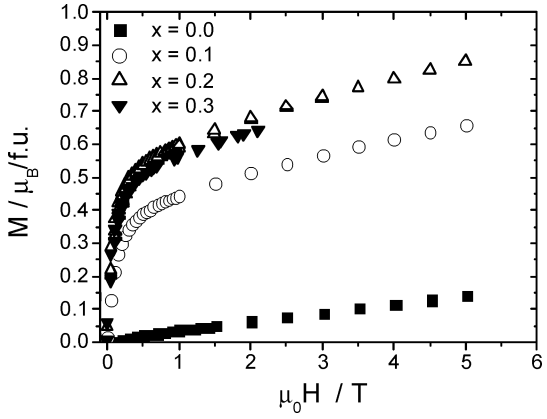


**Figure 7.** Magnetization as a function of applied field for $Ca_4Mn_{3-x}V_xO_{10}$, at 35 K.

**Table 2. Calculated Effective Magnetic Moment, $\mu_{calc}$, and Experimental Values, $\mu_{exp}$ and $\theta$, Obtained from Curie−Weiss Behavior[a]**

| *x* | $\mu_{exp}$ | $\mu_{calc}$ | $\theta$/K |
|---|---|---|---|
| 0 | 4.5 | 3.87 | −592 |
| 0.1 | 3.6 | 3.91 | −111 |
| 0.2 | 4.1 | 3.94 | −107 |
| 0.3 | 4.1 | 3.98 | −104 |

[a] $\mu$ is the effective magnetic moment per manganese ion.

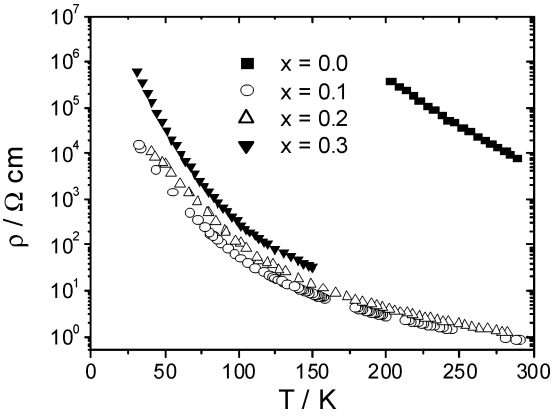


**Figure 8.** Temperature dependence of the electrical resistivity for $Ca_4Mn_{3-x}V_xO_{10}$.

behavior of the inverse dc susceptibility at temperatures above the transition temperature, which shows a negative intercept, $\theta$, with the temperature axis, as expected for the Curie−Weiss behavior of an antiferromagnet. The experimental $\theta$ values and effective magnetic moments are presented in Table 2. The values obtained for $x = 0$ agree with other reported results.[23] For the doped samples the magnetic moments are in good agreement with the values calculated using the expected mixed valence of the Mn ions, and the experimental $\theta$-values are close to the magnetic transition temperatures, contrary to the $x = 0$ case, indicating a more local character of the AFM interactions in the substituted compounds.

The temperature dependence of the electrical resistivity, presented in Figure 8, exhibits for all samples a semiconductor-like behavior, showing no singularity at the magnetic transition temperature. In the case of $x = 0$, the value measured at room temperature is 4 orders of magnitude higher than the values previously reported,[18,23] a difference probably associated with a lower content of oxygen vacan-

(17) Bendersky, L. A.; Greenblatt, M.; Chen, R. *J. Solid State Chem.* **2003**, *174*, 418.
(18) Lago, J.; Battle, P. D.; Rosseinsky, M. J.; Coldea, A. I.; Singleton, J. *J. Phys.: Condens. Matter* **2003**, *15*, 6817.
(19) Battle, P. D.; Blundell, S. J.; Coldea, A. I.; Cussen, E. J.; Rosseinsky, M. J.; Singleton, J.; Spring, L. E.; Vente, J. F. *J. Mater. Chem.* **2001**, *11*, 160.
(20) Battle, P. D.; Green, M. A.; Lago, J.; Millburn, J. E.; Rosseinsky, M. J.; Vente, J. V. *Chem. Mater.* **1998**, *10*, 658.
(21) Girão, A. V.; Carvalho, M. D.; Melo Jorge, M. E.; Costa, F. M., Bonfait, G.; Borges, R. P.; Cruz, M. M.; Godinho, M. *J. Magn. Magn. Mater.* **2004**, *272−276*, E315.
(22) Lago, J.; Battle, P. D.; Rosseinsky, M. J. *J. Phys.: Condens. Matter* **2000**, *12*, 2505.
(23) Mihut, A. I.; Spring, L. E.; Bewley, R. I.; Blundell, S. J.; Hayest, W.; Jestädt, Th.; Lovett, B. W.; McDonald, R.; Pratt, F. L.; Singleton, J.; Battle, P. D.; Lago, J.; Rosseinsky, M. J.; Vente, J. V. *J. Phys.: Condens. Matter* **1998**, *10*, L727.

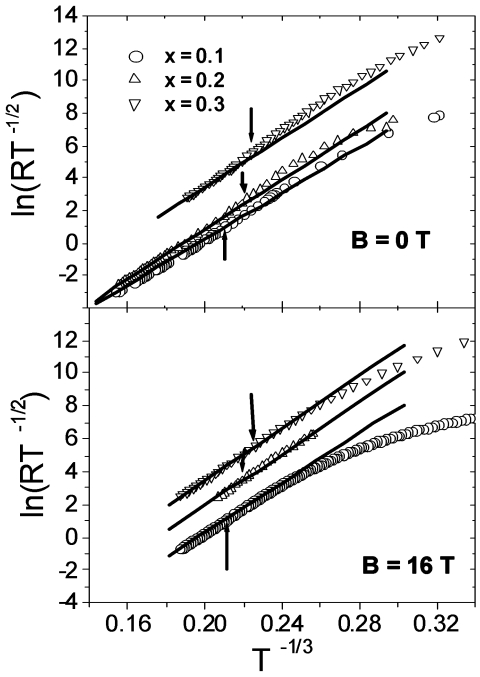


**Figure 9.** Temperature dependence of the electric resistivity for V-doped samples, without applied magnetic field (top) and under an applied field of 16 T (bottom). The representation of $\ln(RT^{-1/2})$ versus $T^{-1/3}$ was chosen to evidence the 2D variable range hopping. The arrows indicate the magnetic transition temperature.

cies. The high resistivity values attained at low-temperature limited our analysis to $T > 200$ K. In this region, the corresponding resistivity can be well-fitted either with polaron hopping or variable range hopping (VRH) models.

For vanadium-doped compounds, the electrical resistivity decreases by 6 orders of magnitude as compared with $x = 0$, and a negative magnetoresistance appears in the ordered state. Nevertheless, the transport behavior remains semiconductor-like. These results are similar to the ones obtained by Raveau and co-workers for the substitution of Mn for $3d^0$ (Nb, Ta, W, Mo) ions in $CaMnO_3$[7] and indicate the existence of ferromagnetic double-exchange interactions.

For the doped samples, the analysis of the resistivity temperature dependence in the range 5 K $< T <$ 300 K, shows a clear separation between the behavior below and above the magnetic transition temperature. Above this temperature, the results are better described by a two-dimensional VRH model (Figure 9), and below this temperature no definite model could be fitted. The 2D behavior, displayed in the paramagnetic region, is consistent with the fact that the conduction is anisotropic in these layered RP phases, the mobility of carriers being higher within the Mn−O planes.[24] The model is parametrized by the characteristic temperature $T_0 = 16\alpha^2/k_B N(E_F)$, where $\alpha$ is the inverse localization length and $N(E_F)$ the density of states at the Fermi level. The determined parameters are presented in Table 3. In the doped samples, the values obtained for $T_0$ are on the order of $4 \times 10^5$ K. For comparison, the same model was fitted for the $x = 0$ sample, resulting in a characteristic temperature $T_0 = 9.3 \times 10^6$ K, higher by a factor of 20. Assuming that the localization length $\alpha$ does not change significantly, the decrease of $T_0$ for the doped samples, when compared with $x = 0$, corresponds to a marked increase in the density of states at the Fermi level, in accordance with the much lower values of the resistivity. For the doped samples, both the electrical resistivity values and the parameter $T_0$ slightly increase with vanadium content. The combination of these results indicates a stronger effect of carrier localization that can be justified by the increasing concentration of $3d^0$ ions ($V^{5+}$) breaking the exchange and conduction paths. The reason no definite model could be used to describe the electrical behavior below the magnetic transition temperature is probably related to the existence of spin-dependent scattering and ionization mechanisms.

(24) Moritomo, Y.; Asamitsu, A.; Kuwahara, H.; Tokura, Y. *Nature* **1996**, *380*, 141.

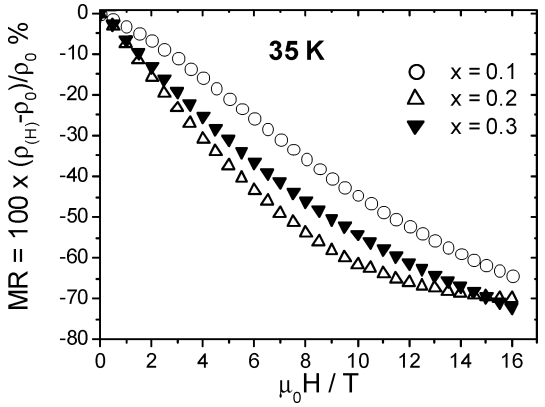


**Figure 10.** Magnetoresistance as a function of magnetic field at 35 K.

**Table 3. Parameter $T_0$ Characterizing the Variable Range Hopping (2D) Behavior, Fitted above the Magnetic Transition Temperature, for the Different Compounds**

| | $T_0/10^5$ K | |
|---|---|---|
| $x$ | $H = 0$ T | $H = 16$ T |
| 0 | 93 | |
| 0.1 | 3.5 | 4.3 |
| 0.2 | 4.5 | 4.9 |
| 0.3 | 4.4 | 5.0 |

To study magnetoresistive effects, the electric resistance was also measured under applied magnetic fields up to 16 T. For all doped samples, the magnetoresistance $[(\rho_H - \rho_0)/\rho_0]$ increases almost linearly with the applied field, attaining values on the order of 70%, in a field of 16 T at 35 K (Figure 10). The negative magnetoresistance can be explained in the same way as in CMR materials. Below the transition temperature without applied magnetic field, the ferromagnetic clusters are randomly oriented and the hopping movement is limited by spin scattering. Under applied magnetic field, the ferromagnetic clusters align, favoring spin-dependent hopping.

Under an applied field, the VRH regime seems to extend to temperatures below the critical temperature while $T_0$ increases in all cases by 10%−20%. This may be explained by a reduction of the density of states at the Fermi level due to the polarization of the intervening electronic states.

## Conclusions

$Ca_4Mn_{3-x}V_xO_{10}$ compounds with $x = 0.1$, 0.2, and 0.3 were successfully synthesized in order to study the effect of electron doping in the Ruddlesden−Popper anisotropic

compounds. The introduction of vanadium in $Ca_4Mn_3O_{10}$ decreases significantly the magnitude of the resistivity and leads to the development of a ferromagnetic component, indicating the existence of a double-exchange mechanism, also confirmed by the negative magnetoresistance exhibited in the magnetically ordered state and explained by the induced mixed valence of manganese. No significant structural modifications were detected, but the low maximum substitution values achieved imply that vanadium affects strongly the chemical stability of the $n = 3$ phase. Doping with pentavalent vanadium affects considerably the electronic distribution.

Semiconducting behavior and antiferromagnetic alignment persist under electron doping, indicating that the appearance of the double exchange interaction does not correspond to the existence of extended electronic states. This result can be explained by considering that $V^{5+}$ ($3d^0$ ion) acts as a positive impurity in the B-sites localizing the $e_g$ electrons.

In conclusion, in the $Ca_4Mn_{3-x}V_xO_{10}$ compounds, vanadium enhances the electrical conduction through electron doping but simultaneously breaks the conductivity paths, preventing metallic behavior. Ferromagnetic character and magnetoresistive effects get stronger upon doping. These characteristics imply that these materials must have polarized carriers and the correlation between the corresponding anisotropic conduction and magnetic polarization may give new ways to control transport in spintronic devices.

**Acknowledgment.** Special thanks are addressed to Dr. Danuta Stroz for EDX measurements. R.P.B. acknowledges FCT (Portugal) for the postdoctoral grant SFRH/BPD/14559/2003. A.V.G. acknowledges FCT (Portugal) for BIC grants supported by the project POCTI/35300/FIS/2000.

CM050395R